Modular Tri-port High-Power Converter for SRM based Plug-in Hybrid Electrical Trucks

Yihua Hu, *Senior Member, IEEE,* Chun Gan, *Member, IEEE,* Qingguo Sun, Peng Li, and Jianhua Wu

***Abstract*—Pug-in hybrid electrical trucks (PHETs) are a kind of emerging transport solution to reduce greenhouse gas emissions. Switched reluctance motors (SRMs) are one of popular choices for PHETs applications due to rear-earth free, high start torque, wide-speed range and fault-tolerance characteristics. Usually, more than two converters are needed to achieve flexible energy conversion between multi electrical energy components on board, i.e., generator, battery bank and motor. High-power converters should be used to drive the trucks that occupy the limited on-board space. Furthermore, an extra converter is also needed to achieve AC grid connecting charging. All those converters make on-board power electronics converter complicated. In this paper, a modular tri-port high-power converter for SRM based PHETs is proposed to combine the multi electrical energy components into one converter. The modular tri-port high-power converter can not only support flexible energy flow, but also support parallel and series winding connection according to the different conditions. Furthermore, AC grid connecting nodes are also developed in the drive, which allows the proposed converter work as a grid connecting charger without extra facilities. The simulation and experimental test rig are employed to verify the feasibility of the proposed converter and corresponding control strategies.**

***Index Terms*—Tri-port, plug-in hybrid electric trucks, SRM, converts, winding connection.**

This manuscript has never been presented at a conference or submitted elsewhere previously.

Yihua Hu is with the Electrical Engineering and Electronics, University of Liverpool, U.K. (E-mail: y.hu35@liverpool.ac.uk)
Chun Gan is with the Department of Electrical Engineering and Computer Science, The University of Tennessee, Knoxville, USA. (E-mail: cgan@utk.edu)
Qinguo Sun is with the College of Electrical Engineering, Zhejiang University, Hangzhou, China. (E-mail: lwsunqg@163.com)
Peng Li is with the Electronic & Electrical Engineering Department, University of Strathclyde, Glasgow, G1 1XW, U.K. (e-mail: peng.li@strath.ac.uk).
Jianhua Wu is with the College of Electrical Engineering, Zhejiang University, Hangzhou, China. (E-mail: hzjhwu@163.com)

I. INTRODUCTION

In recent years, plug-in hybrid electrical trucks (PHETs) have received much attention owing to high demand of fuel-efficient and environment protection against the exhaust gas emission [1]-[5]. PHETs combine the merits of the electrical vehicles and hybrid electrical vehicles, which have a longer running time, flexible grid connection interface and acceptable cost [6]-[9]. Compared to permanent magnet synchronous motors (PMSMs), switched reluctance motors (SRMs) have simple structure with no rotor windings and permanent magnets made from rare-earth materials , and only silicon steel and stator windings are needed. Therefore, these motors have the capability of working for a long time under harsh environment due to their rugged structure [10]-[12]. SRMs also have other advantages such as high efficiency, low cost, good fault tolerance operation, and high starting torque for initial acceleration. Hence, they are considered as a potential candidate for drivetrains of PHETs [13]-[22].

Although, PHETs are promising green transport solution, there are two challenges on electrical energy conversion of PHETs. The first one is on-board high power electrical energy conversion. For series type hybrid electrical vehicle, there are three main electrical energy components including generator, battery bank and driving motor, respectively. In order to optimize operation efficiency, the flexible energy flow among those energy components is needed. For PHETs, an AC-DC converter is also needed to achieve charging function [23]. To equip with those energy conversion functions, at least two power electronics converters are needed to link the generator, battery bank and SRM. For example, a DC-DC converter is needed to connect battery bank with generator and motor [24]. However, the on-board space is limited, the bus voltage control and coordination control of converters also increase the control complexity and decrease the reliability of the on-board energy conversion equipment. Therefore, it is important to integrate all the converters together to give more compact solution for on-board energy conversion [25]. The other challenge is AC grid-connected charging [26]-[28]. The massive construction of charging stations not only occupies limited city land, but also needs large funding investment and carefully chose location that impedes the wide application of PHETs [29]-[31].

Aim to deal with those two challenges, several solutions have been tried. In [32], the switched reluctance motor operates under AC mains or a low voltage battery supply by using the proposed circuit. The motor also can be utilized as the voltage-changing transformer without increasing the system cost. For the EVs application background, by integrating a bidirectional AC-DC charger with the DC-DC converter, the on-board energy conversion can be simplified [33]. In this case, the charging system can control energy flow between the high voltage bus and the battery bank. However, its circuitry is complicated and the available power flow modes are limited. An integrated driving/charging SRM drive for EVs is presented in [34]. The Miller converter and the fronted DC-DC boost converter are constructed by using two intelligent power modules (IPMs), which can improve the driving performance by adopting the proper control strategies. In order to reduce the cost and weight effectively for hybrid vehicles, a new concept is proposed to integrate the DC-DC converter functionality into the traction drive system [35], in which the inverter and the

machine can be utilized to implement a primary bridge leg of an isolated full-bridge DC-DC converter. In [36], a converter is presented to combine motoring and charging functions. However, an auxiliary winding must be used to closely couple to one SRM phase winding, which increase the complexity and inconvenience for the system. Multiphase induction machine and its driving topology is employed to achieve charging without charging station function, while the stator structure should be changed and switching devices number is triple compared with the traditional induction machine [37]. Split-phase technology has been used in permanent-magnet (PM) machine. A 20 kW PM motor drive is specially designed and its traction/charging modes are controlled by a switch based relay [38], but the motor suffers from high harmonic contents in the back electromotive force (EMF). For SRM based EV, charging without charging station technology has been explored. A 2.3kW SRM in [39] with an asymmetrical half-bridge converter can provide on-board charging and power factor correction functions for EVs application background. However, a boost-type front-end DC-DC converter is externally equipped, making this topology less practical and flexible for the target application. In summary, the current technologies cannot give the approving solutions to the proposed challenges, because there are mainly two drawbacks in current technologies for the PHET applications.

(1) The state-of-the-art on-board converters only achieve converter integration for the electrical vehicles (EVs) applications background; while for the PHETs application, more energy components are on board; no integration converter has been reported yet, which combine generator, battery bank and motor in one converter and also support flexible energy flow. Especially for high power level background, no solutions have been reported yet.

(2) Charging without charging station technology has been explored in induction machines, PMSMs and SRMs. While, either complicate motor structure or complicate power electronics topology is used to achieve grid-connection function.

Consequently, current technologies have not given the overall resolution scheme for on-board high power tri-port converter of PHETs to conquer the two challenges at the same time. This paper is set out to fill the gap by proposing a new integrated tri-port converter for SRM based PHETs. In this paper, the proposed converter for PHETs is illustrated in section II; and the corresponding control strategies are presented in the section III; simulation and experiments are also carried out to verify the proposed topology in section IV. The conclusion is given at final part.

II. Proposed Tri-port Converter and Operation Modes

2.1 Proposed Tri-port Topology

The proposed tri-port topology for three-phase 12 slots 8 poles SRM based PHET is presented in Fig.1. A1, A2, A3 and A4 are the phase A windings. N_{a1} and N_{a2} are the AC grid connecting points, and S_1~S_8 are the Insulated Gate Bipolar Transistors (IGBTs). Phase B and phase C have the same topology with phase A. The proposed topology has modular structure that is convenient for

massive production. Two single phase inverters are employed for each phase. Compared with the traditional asymmetrical half-bridge driving topology for SRM, the proposed converter is easier to manufacture.

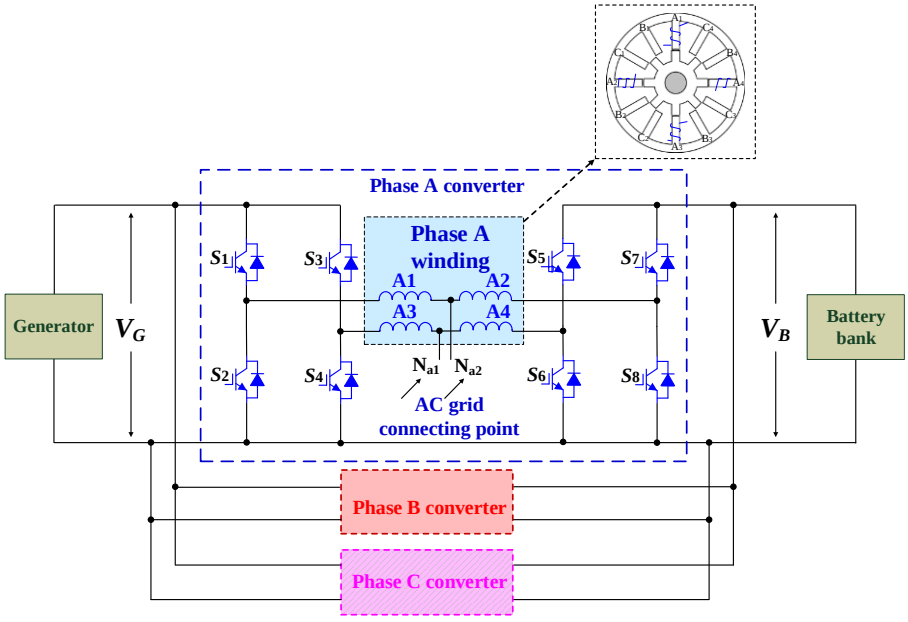

Fig.1 Proposed tri-port high power SRM driving topology.

2.2 Topology working states

As illustrated in Fig.2, there are five typical working scenarios for PHET, which are starting, low speed running, accelerating, high speed running and braking, respectively. For different working scenarios, the corresponding energy components should cooperate to achieve flexible energy flow. According to the working scenarios, there are different working states to support energy flow modes in the proposed converter. The following part will introduce the proposed topology working for different scenarios.

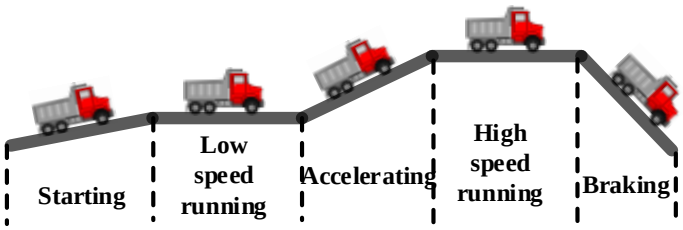

Fig. 2. Typical PHET working scenarios.

2.3 One source driving mode with series winding connection

Phase winding connected in series is a traditional driving mode for SRM operation. For example, in phase A, the windings A1, A2, A3 and A4 are connected in series, as shown in Fig.3. When turn on S_1, S_3, S_5 and S_8, the battery bank supplies energy to the windings, as illustrated in Fig.3 (a). When turn on S_1, S_3, S_6 and S_7, windings energy is recycled to battery bank, as shown in Fig.3 (b). By conducting S_1, S_3, S_5, and S_7, the motor is in the freewheeling state, as shown in Fig.3 (c). Except battery bank supplying

energy to the motor, the generator also can supplies energy to the motor; when turn on S_1, S_4, S_5 and S_7, the generator supplies energy to the windings, as illustrated in Fig.3 (d). When turn on S_2, S_3, S_5, and S_7, windings energy is recycled to generator, as illustrated in Fig.3 (e). The motor also can work in freewheeling state as presented in Fig.3 (c). For one source driving mode with series winding connection, the PHETs can work at low speed running.

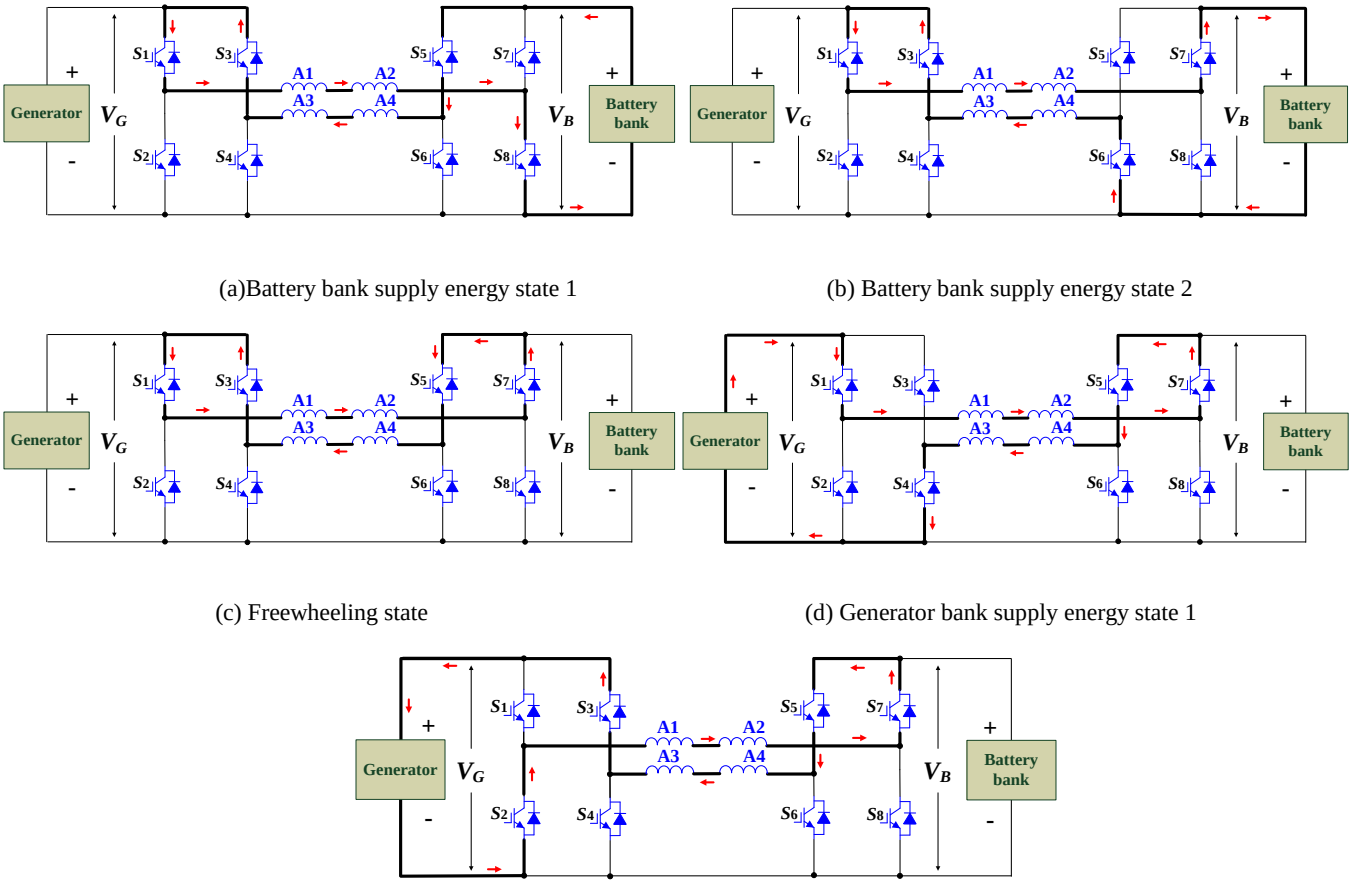

(a)Battery bank supply energy state 1

(b) Battery bank supply energy state 2

(c) Freewheeling state

(d) Generator bank supply energy state 1

(e) Generator bank supply energy state 2

Fig. 3 Series winding connection driving mode.

2.4 One source driving mode with parallel winding connection

The proposed topology also can support SRM working at parallel winding connection mode. In phase A, the winding A1 and A2 are connected in series; A3 and A4 are connected in series; windings A1 and A2 are parallel with windings A3 and A4. When turn on S_1, S_3, S_6 and S_8, the generator supplies energy to the windings, as illustrated in Fig.4 (a). When turn on S_2, S_4, S_5 and S_7, windings energy is recycled to battery bank, as shown in Fig.4 (b). By conducting S_2, S_4, S_6 and S_8, the motor is in the freewheeling state, as shown in Fig.4 (c). In parallel driving mode, the energy supply source and energy recycling source are different. This can be employed as tri-port energy conversion. As shown in Fig.4, the energy from generator delivers to SRM and battery bank at the same

time. Furthermore, due to phase winding in parallel, the equivalent phase inductance is lower than series connection and the corresponding phase current increases faster. For one source driving mode with parallel winding connection, the PHETs can work at high speed running.

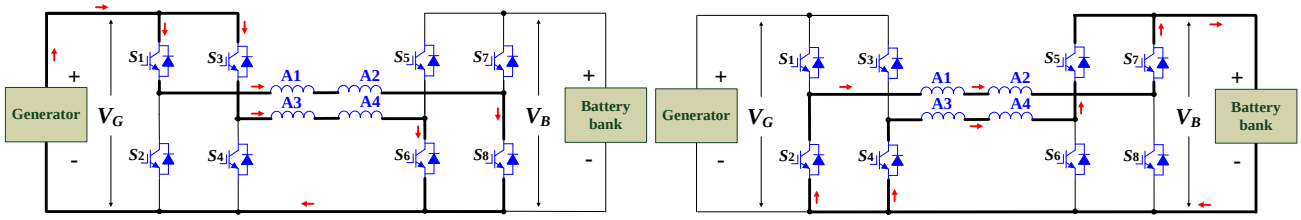

(a) Excitation state under parallel driving mode

(b) Energy recycling under parallel driving mode

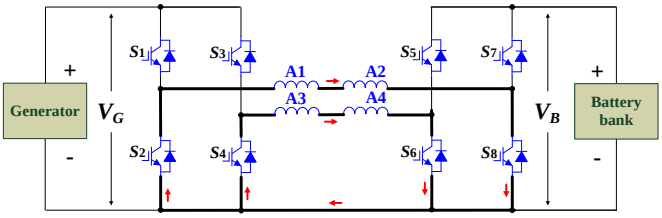

(c) Freewheeling state under parallel driving mode

Fig. 4 Parallel winding connection driving mode.

2.5 Dual source driving mode

By controlling switching devices, both generator and battery bank can supply energy to motor. As shown in Fig.5 (a), turn on S_2 and S_7, the battery bank supplies energy to windings A1 and A2; turn on S_3, S_6, the generator supplies energy to windings A3 and A4. When V_G equals V_B, the whole circuit can be equivalent to that the generator and the battery bank connected in series supply energy to series windings A1~ A4. As shown in Fig.5 (b), turn on S_1, S_8, the energy in windings A1 and A2 is recycled to generator; turn on S_4 and S_5, the energy in windings A3 and A4 is recycled to battery bank. When turn on S_2, S_4, S_5 and S_7, the windings are in freewheeling state, as shown in Fig.5 (c). For dual source driving mode, the PHET can output maximum power that supports PHET starting and accelerating scenarios. In this working mode, the phase current can be built in a short time which can be employed in PHET breaking mode.

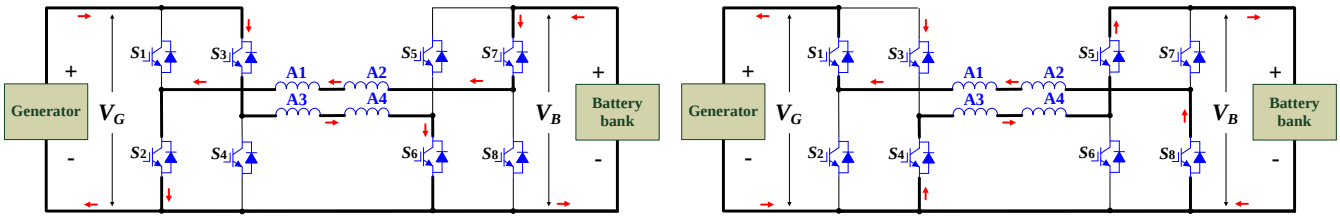

(a) Excitation state under dual source driving mode

(b) Energy recycling under dual source driving mode

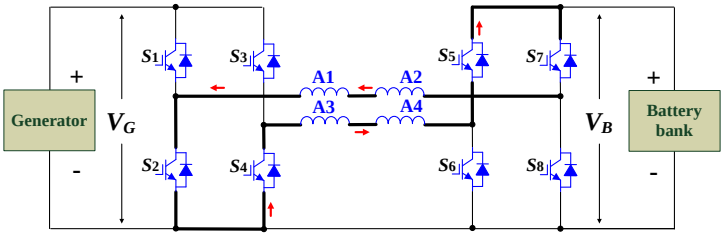

(c) Freewheeling model under dual source driving mode

Fig.5 Dual source driving mode.

2.6 Tri-port driving mode

When the output power of the generator is higher than the need of motor, the tri-port driving mode can be employed to achieve energy balance. Both series winding connection working mode and parallel winding connection working mode can support tri-port driving mode.

When the proposed converter is in series working mode, the generator can supply energy to SRM and battery bank at the same time. The corresponding excitation state is the same as Fig.3 (d). During this state, the generator supplies energy to generate torque. The energy recycling state is the same as Fig.3 (b). During the recycling state, the battery bank is charged by the energy from the phase winding storage. Therefore, the motor driving and battery charging can be simultaneously achieved.

When the proposed converter is in parallel working mode, the generator can also supply energy to SRM and battery bank at the same time. In this driving mode, the excitation state is the same as Fig.4 (a), in which the generator supplies energy to phase windings. And then, the energy recycling state is shown in Fig.4. (b), in which, the windings energy is recycled to the battery bank.

A. Energy charging/discharge between generator and battery

When PHET is in standstill mode, the battery bank needs to be charged. In this scenario, the proposed converter can work as a DC-DC converter. The converter working states are the same as the winding parallel connecting driving mode (Fig.4 (a)~(c)). When PHET needs to start ICE, in the proposed converter, the battery bank can supply energy to generator/starter, which is similar to that the generator supplies energy to the battery bank.

B. AC Grid charging

The proposed converter can connect with power grid directly to charge the battery bank. The central tapped nodes N_{a1} and N_{a2} can be employed to connect with power grid. The corresponding four working states are presented in Fig. 6 (a)~(d).

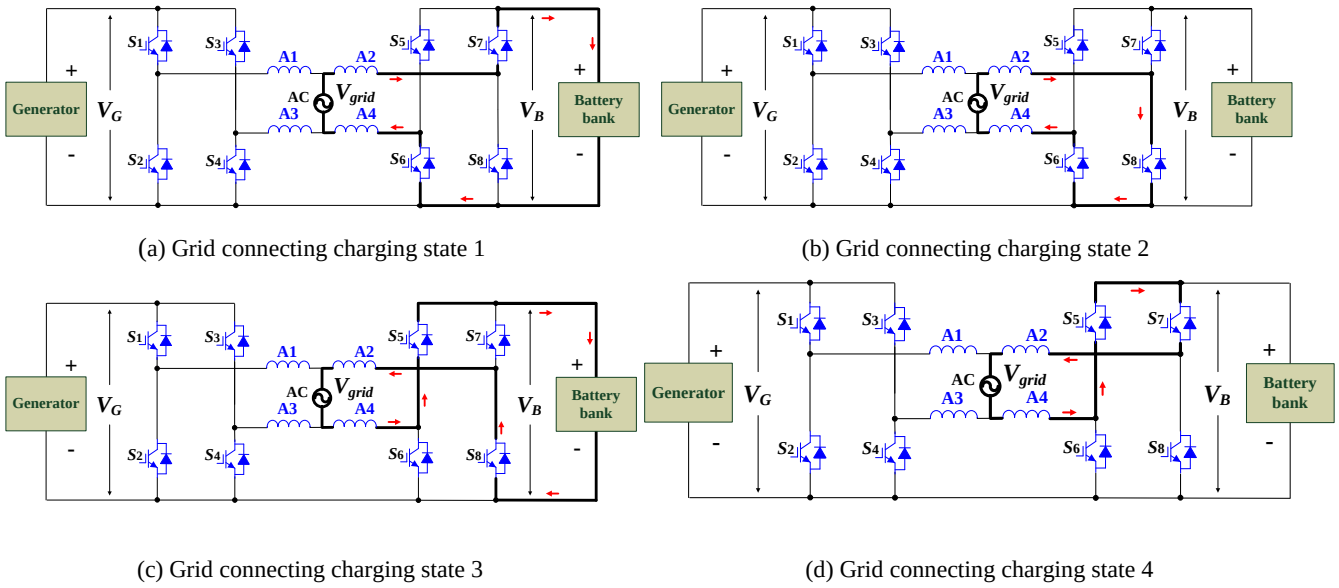

(a) Grid connecting charging state 1

(b) Grid connecting charging state 2

(c) Grid connecting charging state 3

(d) Grid connecting charging state 4

Fig.6 Grid connecting charging.

For high power charging, three phase AC grid connecting also can be realized by connecting N_{a1} and N_{a2} together to form charging point N_{a12}. Similar grid connecting charging points N_{b12} and N_{c12} can be formed, as shown in Fig. 7.

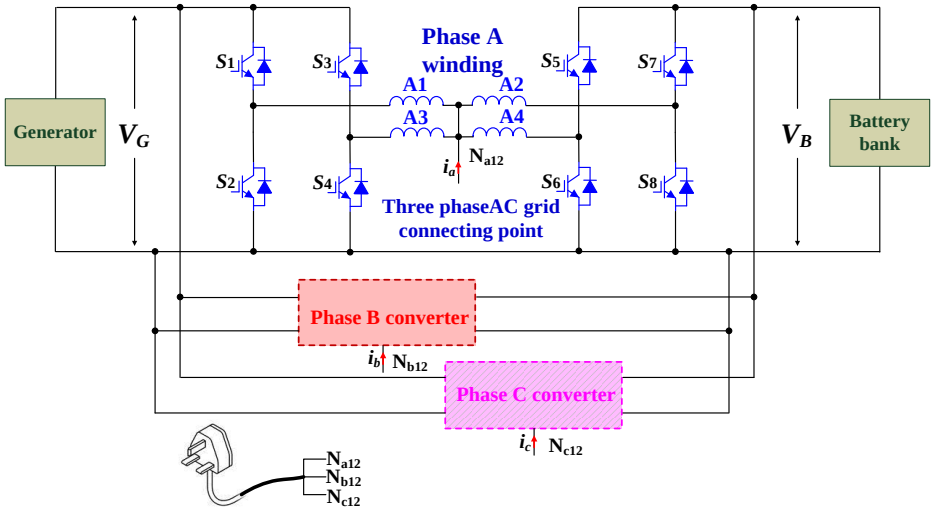

Fig. 7 Three phase AC grid charging connecting.

2.7 Comparison with the state-of-the-art tri-port topologies

In the proposed topology, although the total solid state devices number is increased compared with traditional asymmetrical half bridge topology, the voltage stress of solid state devices is decreased by the decentralized topology, which will benefit from the cooling design; the standard full bridge module structure makes the proposed converter easy and low cost to massive produce. In paper [40], a high power level DC-DC converter is employed connect the battery bank with DC bus in the hybrid powertrain, which needs a lot of solid state devices and passive components, while in the proposed tri-port topology, the battery bank, generator and motor are combined in one converter. Therefore, the total solid state devices number is not increased obviously. Table I is the

comparison of proposed converter with other tri-port converter, which illustrates the merits of the proposed converter with the-state-of-art converters.

TABLE I THE PROPOSED TOPOLOGY COMPARING WITH OTHER TRI-PORT CONVERTERS

	Proposed method	Topology in [3]	Topology in [41]
Power level	High	Low	Medium
Energy flow flexibility	High	Low	Medium
Fault tolerance	Achievable without phase absence	Without fault tolerance	Without fault tolerance
Modular structure	Yes	No	No
Grid connecting charging	Without charging station	Need charging converter	Need charging converter

III. CONTROL STRATEGY FOR THE PROPOSED TRI-PORT CONVERTER

In order to control the proposed converter in different working modes, this section illustrates the control strategies for driving and charging modes.

3.1 Modeling of SRM with different winding connecting modes

Considering that the complicated electromagnetic characteristic due to the double salient structure for SRMs, the linear mathematical model of SRMs is adopted for the convenient analysis. Under the hypothesis of linear model, the profiles of phase inductance and phase current in the different rotor position are illustrated in Fig. 8, where i is the phase current; L is the phase inductance; θ_{on} and θ_{off} are the turn-on and turn-off angles, respectively. The phase inductance increases linearly from the unaligned position θ_2 to the aligned position θ_3, and the phase current can decrease to zero in the rotor position $\theta=\theta_4$.

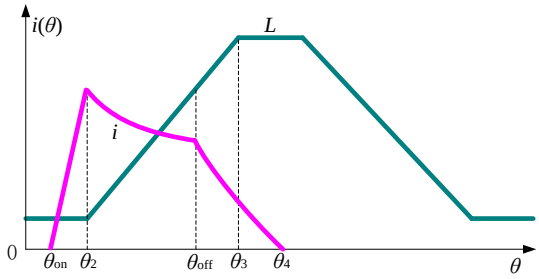

Fig. 8. Profiles of phase inductance and phase current.

The phase current in the different conduction region can be expressed as

$$i_k(\theta)=\begin{cases}\dfrac{U_{in}}{\omega_r}\dfrac{\theta-\theta_{on}}{L_{\min}}, & \theta_{on}\le\theta<\theta_2\\ \dfrac{U_{in}}{\omega_r}\dfrac{\theta-\theta_{on}}{L_{\min}+K(\theta-\theta_2)}, & \theta_2\le\theta<\theta_{off}\\ \dfrac{U_{in}}{\omega_r}\dfrac{2\theta_{off}-\theta_{on}-\theta}{L_{\min}+K(\theta-\theta_2)}, & \theta_{off}\le\theta<\theta_3\\ \dfrac{U_{in}}{\omega_r}\dfrac{2\theta_{off}-\theta_{on}-\theta}{L_{\max}}, & \theta_3\le\theta<\theta_4\\ 0, & others\end{cases} \tag{1}$$

where $L_{\min}$ and $L_{\max}$ are the minimum and maximum of the phase inductance, and K is the slope factor of the phase inductance.

The phase current reaches its peak value at the position $\theta=\theta_2$, which is expressed as

$$i_{max}=\frac{U_{in}}{\omega_r}\frac{\theta_2-\theta_{on}}{L_{\min}} \tag{2}$$

The instantaneous torque of the phase k is

$$T_k=\begin{cases}0, & \theta_{on}\le\theta<\theta_2\\ \dfrac{1}{2}Ki_k^{\,2}, & \theta_2\le\theta<\theta_3\\ 0, & \theta_3\le\theta<\theta_4\end{cases} \tag{3}$$

For the proposed tri-port topology, the branch inductance will be half of its original under the winding parallel and dual source driving modes, which cause the slope factor to be reduced by half. According to (1) and (2), the current peak value of each parallel branch will be twice as the one under the winding series driving mode due to the inductance decrease. For the conventional single pulse-APC and voltage-PWM control strategies, the increment of current peak value will bring a series of unexpected consequence, such as low efficiency and high torque ripple. In order to diminish the negative influence caused by the wingding parallel connection, the proper hysteresis of the turn-on angle is necessary, which can be shown in Fig. 9. $i'$and L' are the branch current and branch inductance under the winding parallel and dual source driving modes, and i'' is the current after adjusting the turn-on angle. In the current chopping control (CCC) scheme, this is not to considerate because the current is the direct control variable and the peak value would not exist.

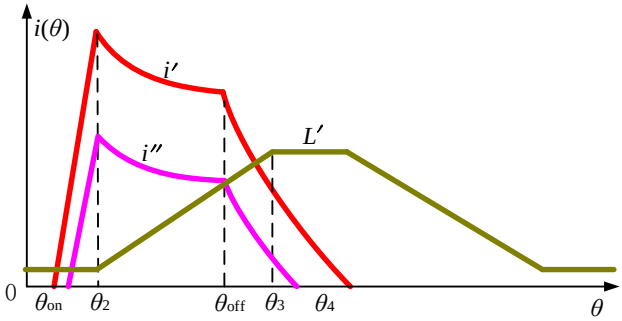

Fig. 9. Turn-on angle under APC and PWM schemes.

According to (3), the instantaneous torque of each branch, under the winding parallel and dual source driving modes, will be reduced by half under the same current, which can be realized by adjusting the turn-on angle. Therefore, the total torque of each phase in the different modes will be similar, which is given by

$$T_{k12} = \frac{1}{2} K' {i_{k12}}^2 = \frac{1}{2} \times \frac{1}{2} K {i_{k12}}^2 = \frac{1}{4} K {i_{k12}}^2 \tag{5}$$

$$T_{k34} = \frac{1}{2} K' {i_{k34}}^2 = \frac{1}{4} K {i_{k34}}^2 \tag{6}$$

$$T_k' = T_{k12} + T_{k34} = \frac{1}{2} K {i_k}^2 = T_k \tag{7}$$

where K' is the slop factor of each branch inductance under the winding parallel and dual source driving modes; T_{k12} and T_{k34} are the instantaneous torque of each branch; T_k' is the total torque of kth winding.

3.2 *Control strategy for driving mode*

When the proposed tri-port converter is in SRM driving mode, the topology of the system is the same as the traditional asymmetrical half bridge topology; the voltage-PWM control and current chopping control (CCC) are adopted as two basic control schemes. According to the given speed ω^*, the controller works in CCC strategy under low speed condition, and the controller works in voltage-PWM control strategy under high speed condition. The whole control block diagram is presented in Fig.10. The classical proportional integral (PI) algorithm is used in speed controller to regulate the SRM speed. Encoder gives the SRM rotor position information and the corresponding motor speed can be calculated by a micro-controller. The turn-on and turn-off angles of SRM are determined by a commutation controller. In the CCC strategy, the phase current is the control variable. The real time phase current is measured by current sensor; and the phase current reference i^* is derived from the speed controller. The hysteresis controller is employed to generate the driving signal for switching devices. In the voltage-PWM control system, the phase voltage is the control variable. According to the speed error, the effective phase voltage is controlled by the duty ratio of the switching signal.

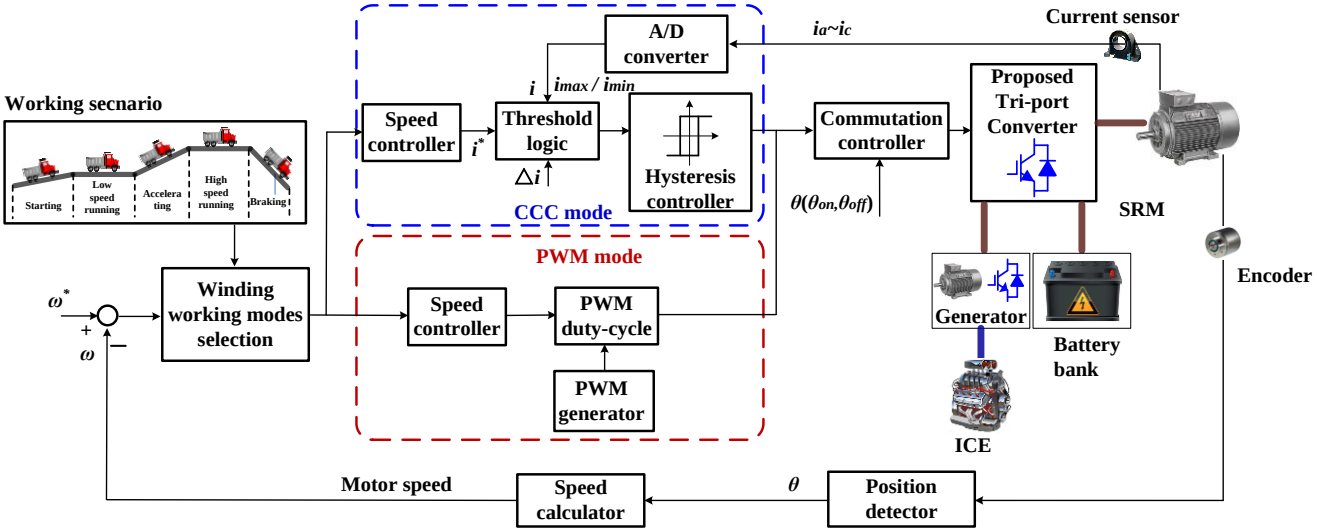

Fig. 10. SRM control strategy under driving mode.

3.3 Control strategy for charging

Battery bank to generator (B-G) and generator to battery bank (G-B) are the standstill energy exchange mode. When PHET is in standstill battery charging mode (G-B) or generator starting (B-G) mode, the proposed tri-port converter needs to work as a DC-DC converter to transfer energy between the generator and battery bank. In order to achieve high power level, three phases drive converter can work in parallel mode. The corresponding control block diagrams are illustrated in Fig. 11. In the constant voltage control, the current reference is calculated from the output voltage error in the proportional-integral (PI) control loop.

Due to dual salient structure of SRMs, the phase inductance is changed with rotor position. Therefore, the uncertainty of phase inductance makes difficult to apply common control methods such as vector control (*d-q* decoupling). In order to mitigate the influence of uncertainty and unbalance of phase inductor, hysteresis control strategy is proposed, as shown in Fig.11. $S_{5'}$, $S_{6'}$, $S_{7'}$ and $S_{8'}$ are the switching devices of Phase B converter; similarly $S_{5''}$, $S_{6''}$, $S_{7''}$ and $S_{8''}$ are the switching devices of Phase C converter; PLL is the phase lock loop to get three phase sine signal; i_a, i_b and i_c are the input current of phase A, B and C, respectively.

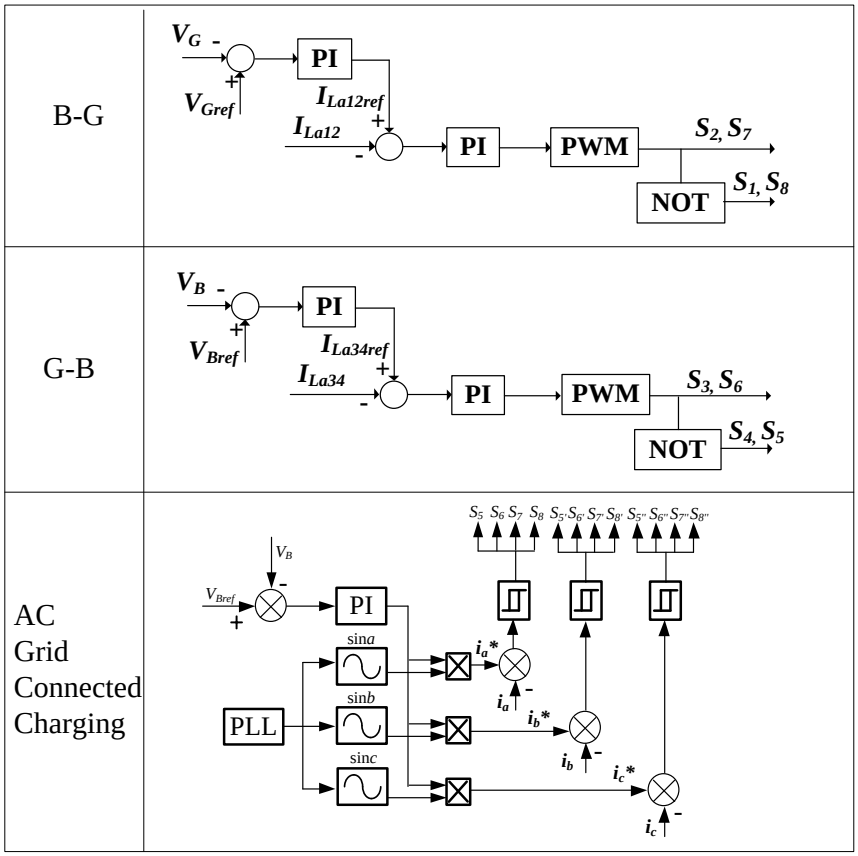

Fig. 11. Control strategy for charging.

IV. Experiment Verification

In order to verify the proposed modular tri-port converter for SRM based PHET, the experiments are carried out. A low-power three-phase 12/8 prototype SRM is employed for proof-of-concept. Fig. 12 shows the experimental rig based on a 750W SRM, where the motor parameters are illustrated in Table II. A dSPACE-DS1006 control platform is employed as the main controller, which is used to realize the control algorithm. The SRM is driven by the proposed tri-port converter and a Parker AC servomotor acts as the load. A 48V lead-acid battery bank acts as the power supply. The phase currents are obtained by three Hall-effect current sensors. A speed sensor and a torque sensor with high sensitivity and wide dynamic range are employed to measure the information of the motor speed and instantaneous torque.

TABLE II Motor Parameters

Parameters	Value
Phase number	3
Stator poles	12
Rotor poles	8
Rated speed (r/min)	1500
Rated power (W)	750
Phase resistor (Ω)	3.01
Minimum phase inductance (mH)	27.2
Maximum phase inductance (mH)	256.7
Rotor outer diameter (mm)	55
Rotor inner diameter (mm)	30

Stator outer diameter (mm)	102.5
Stator inner diameter (mm)	55.5
Core length (mm)	80
Stator arc angle (deg)	14
Rotor arc angle (deg)	16

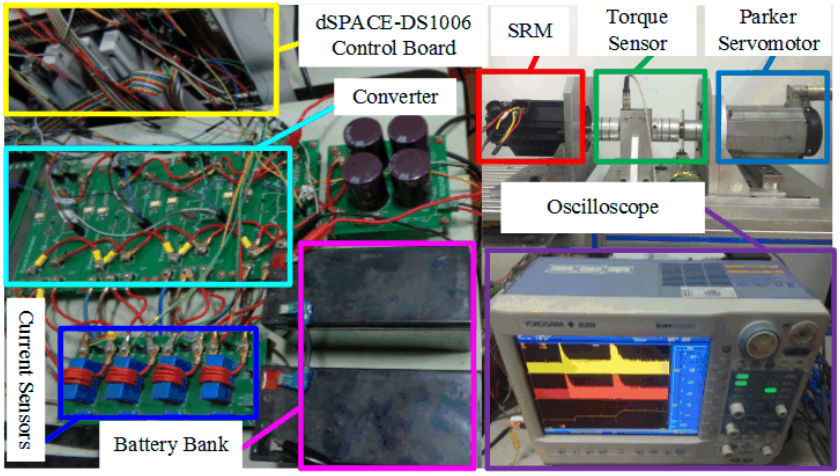

Fig. 12. Experimental setup.

Fig. 13 illustrates the experimental results when the motor works in series winding connection driving mode under CCC and PWM schemes, where the turn-on angle is set to 0 °and the turn-off angle is 22 °. In the waveforms, i_a, i_b, and i_c are the currents of three phases, and U_{12} is the voltage of the phase winding A1 and A2. Fig. 13 (a), (b) and (c) show the operation states at 300 rpm and 800 rpm, respectively, under CCC scheme, where the motor is supplied energy by the battery bank. Fig. 13 (d), (e) and (f) show the waveforms under PWM scheme, and the energy is also supplied by the battery bank. As shown in the figures, the voltage of half of the phase-A wingding is 24 V. When the generator provides the energy to the motor under the two control strategies, the corresponding waveforms are similar to Fig. 13. The operation of the proposed drive system during acceleration is shown in Fig. 13 (c) and (d) under the two control scheme. As illustrated in the figures, the speed follows the given value well during the continuous acceleration progress.

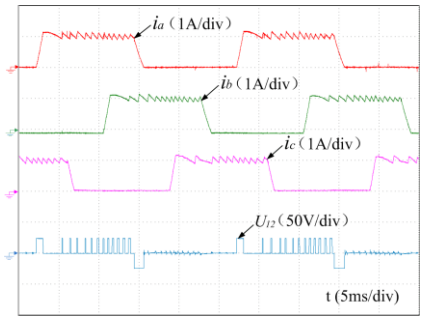

(a) 300 rpm under CCC scheme

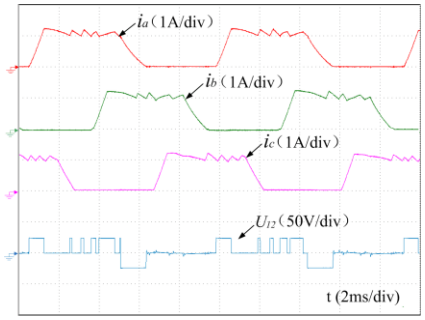

(b) 800 rpm under CCC scheme

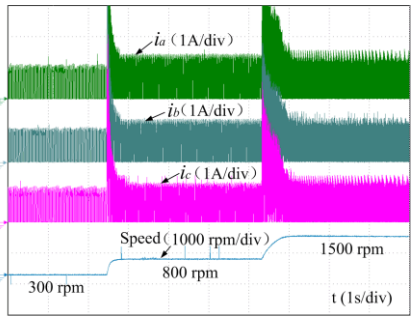

(c) Acceleration operation under CCC scheme

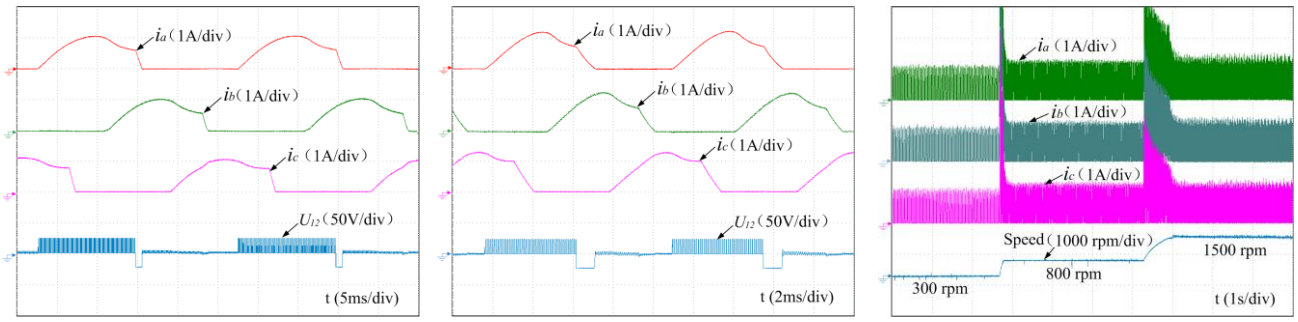

(d) 300 rpm under PWM scheme (e) 800 rpm under PWM scheme (f) Acceleration operation under PWM scheme

Fig. 13. Experimental results under windings series driving mode.

Fig. 14 illustrates the waveforms when the motor works in the parallel winding connection driving mode, where i_{a12} is the branch current consisting of phase winding A1 and A2, and i_{a34} is the branch current of phase winding A3 and A4. Fig. 14 (a), (b) and (c) show the waveforms at 300 and 800 rpm under CCC scheme. Fig. 14 (d), (e) and (f) show the waveforms at 300 and 800 rpm under PWM scheme. The energy is provided by the generator, and the voltage of each branch is the bus voltage 48 V. When the switches S_2, S_4, S_5 and S_7 are turned on, the winding energy from the two branch of each phase is recycled to the battery bank.

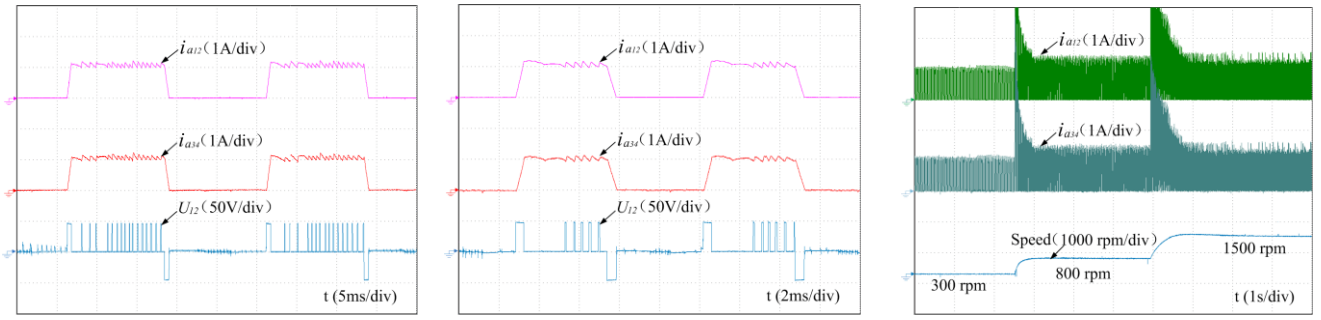

(a) 300 rpm under CCC scheme (b) 800 rpm under CCC scheme (c) Acceleration operation under CCC scheme

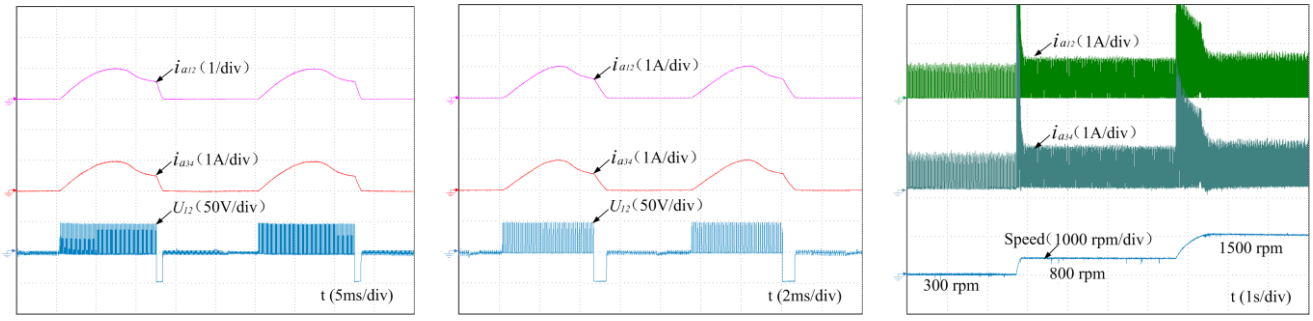

(d) 300 rpm under PWM scheme (e) 800 rpm under PWM scheme (f) Acceleration operation under PWM scheme

Fig. 14. Experimental results under windings parallel driving mode.

Fig. 15 illustrates the experimental waveforms under dual source driving mode, where the voltage of each branch is also the bus voltage 48 V. The branch consisting of phase winding A1 and A2 is supplied energy by the battery bank when the switches S_2 and S_7 are turned on, and the winding energy is fed back to generator when the switches are both turned off. The branch consisting of phase winding A3 and A4 is supplied energy by the generator when the switches S_3 and S_6 are turned on, and the winding energy is recycled to the battery bank by turning off both switches. Compared with the parallel winding connection driving mode, the current direction of the two branches are opposite under dual source driving mode.

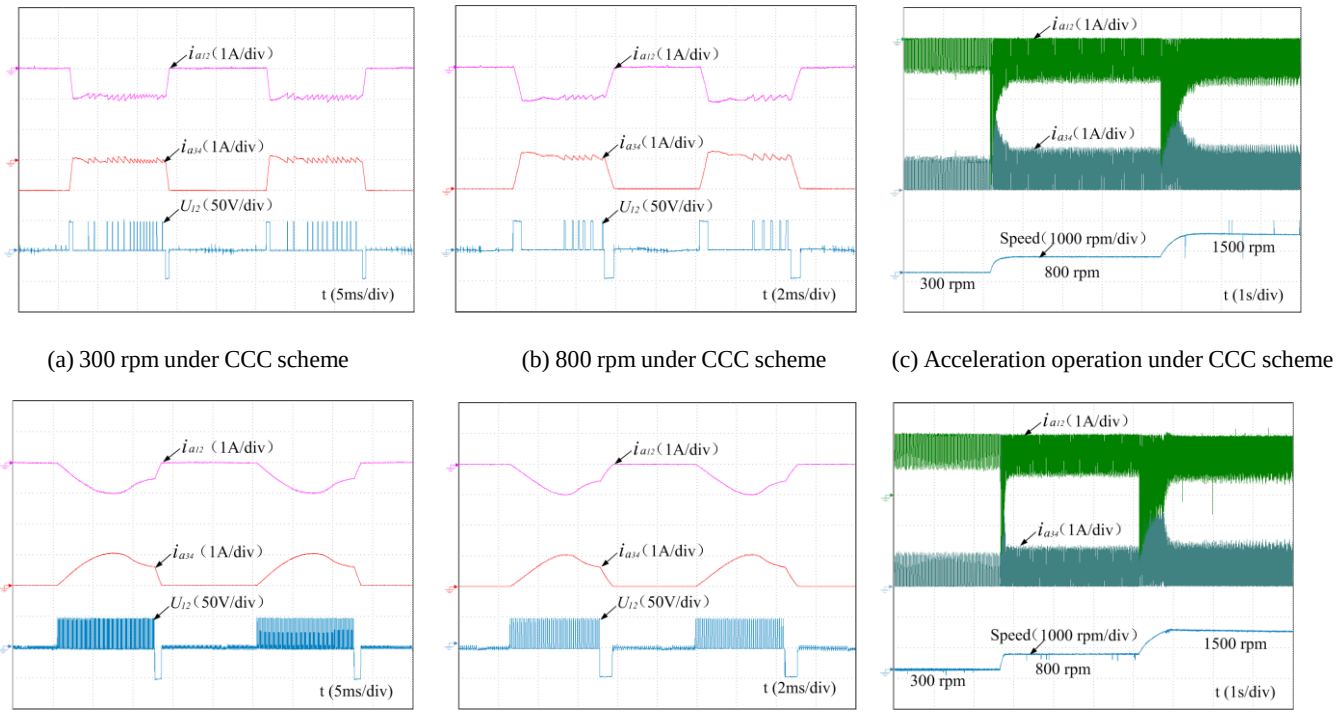

(a) 300 rpm under CCC scheme (b) 800 rpm under CCC scheme (c) Acceleration operation under CCC scheme

(d) 300 rpm under PWM scheme (e) 800 rpm under PWM scheme (f) Acceleration operation under PWM scheme

Fig. 15. Experimental results under dual source driving mode.

Fig.16 presents the current waveforms under programmable three phase AC source connected charging tests. In Fig. 16, V_z is the rotor position sensor output, which keeps at zero. Because of the dual salient and symmetrical structure of the motor, the tangential force of the rotor is balanced when the three phase windings are excited simultaneously. Therefore, the SRM can keep standstill during the charging progress. By employing the hysteresis control strategy, phase current is also with high quality waveforms and the corresponding total harmonic distortion (THD) is 3.1%. Fig.17 gives the experimental results for standstill mode charging (generator to battery). The difference of the phase current waveform is caused by the phase inductance difference.

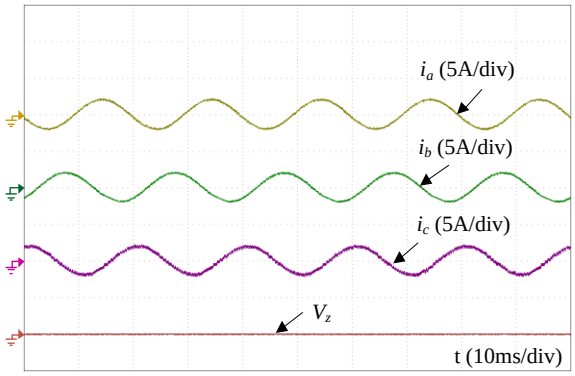

Fig. 16 Waveform of grid connected three phase AC charging.

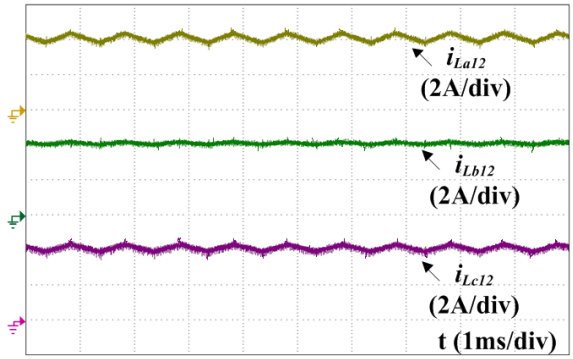

Fig.17 Experimental results for standstill energy exchange mode.

V. CONCLUSION

SRM has been employed as the motor for the PHET application in this paper. In order to achieve flexible energy flow control of PHET, this paper has proposed a tri-port converter with modular and concise structure to combine a generator, a battery bank and a SRM into one converter; and the corresponding working modes and control strategies are investigated in details. The main contributions of this paper are:

(i) The proposed tri-port converter combines three on-board energy components together. The proposed converter is with the characteristics of high power level, modular structure that supports massive production.

(ii) A novel tri-port high power convert for PHET is proposed that supports flexible energy flow control. Under driving condition, the proposed topology supports five energy flow modes including generator to SRM, battery bank to SRM, generator and battery bank to SRM, generator to SRM and battery bank, and battery bank to SRM and generator; under standstill condition, the proposed topology supports two energy flow modes including generator to battery bank, battery bank to generator.

(iii) In order to cooperate with the six working modes, the corresponding control strategies are developed to achieve flexible energy flow control.

REFERENCES

[1] K. J. Dyke, N. Schofield, and M. Barnes，"The impact of transport electrification on electrical networks," *IEEE Trans. Ind. Electron.*, vol. 57, no. 12, pp. 3917- 3926，Dec. 2010.

[2] B. K. Bose, "Global energy scenario and impact of power electronics in 21st century," *IEEE Trans. Ind. Electron.*, vol. 60, no. 7, pp. 2638-2651, Jul. 2013.

[3] Y. Hu, X. Song, W. Cao, and B. Ji, "New SR drive with integrated charging capacity for plug-in hybrid electric vehicles (PHEVs)," *IEEE Trans. Ind. Electron.*, vol. 61, no. 10, pp. 5722-5731, Oct. 2014.

[4] B. Ji, X. Song, W. Cao, V. Pickert, Y. Hu, J. W. Mackersie, and G. Pierce, "In situ diagnostics and prognostics of solder fatigue in IGBT modules for electric vehicle drives," *IEEE Trans. Power Electron.*, vol. 30, no. 3, pp. 1535-1543, Mar. 2015.

[5] S. Morimoto, O. Shohei, Y. Inoue, and M. Sanada, "Experimental evaluation of a rare-earth-free PMASynRM with ferrite magnets for automotive applications," *IEEE Trans. Ind. Electron.*, vol. 61, no. 10, pp. 5749-5756, Oct. 2014.

[6] S. S. Williamson; A. K. Rathore; F. Musavi, "Industrial electronics for electric transportation: current state-of-the-art and future challenges," *IEEE Trans. Ind. Electron.*, vol. 62, no. 5, pp. 3021 - 3032, May. 2015.

[7] C. C. Chan, Alain Bouscayrol, and Keyu Chen, "Electric, hybrid, and fuel-cell vehicles: architectures and modeling, " *IEEE Trans. Veh. Technol.*, vol. 59, no. 2, pp 589-598, Feb. 2010.

[8] O. C. Onar, J. Kobayashi, and A. Khaligh, "A fully directional universal power electronic interface for EV, HEV, and PHEV Applications," *IEEE Trans. Power Electron.*, vol. 28, no. 12, pp. 5489-5498, Dec. 2013.

[9] S. Dusmez, and A. Khaligh, "A compact and integrated multifunctional power electronic interface for plug-in electric vehicles," *IEEE Trans. Power Electron.*, vol. 28, no. 12, pp. 5690-5701, Dec. 2013.

[10] Miller T. J. E. "Switched reluctance motors and their control," London: Magna Physics Publishing and Oxford Science, 3-25, 1993.

[11] J. Ye, B. Bilgin, and A. Emadi, "An extended-speed low-ripple torque control of switched reluctance motor drives," *IEEE Trans. Power Electron.*, vol. 30, no. 3, pp. 1457-1470, Mar. 2015.

[12] W. Cai, and F. Yi, "An Integrated Multiport Power Converter With Small Capacitance Requirement for Switched Reluctance Motor Drive," *IEEE Trans. Power Electron.*, vol. 31, no. 4, pp. 3016-3026, Apr. 2016.

[13] K. Kiyota, T. Kakishima, and A. Chiba, "Comparison of test result and design stage prediction of switched reluctance motor competitive with 60-kW rare-earth PM motor," *IEEE Trans. Ind. Electron.*, vol. 61, no. 10, pp. 5712-5721, Oct. 2014.

[14] Y. Hu, X. Song, W. Cao, and B. Ji, "New SR drive with integrated charging capacity for plug-in hybrid electric vehicles (PHETs)," *IEEE Trans. Ind. Electron.*, vol. 61, no. 10, pp. 5722-5731, Oct. 2014.

[15] K. M. Rahman, B. Fahimi, G. Suresh, A. V. Rajarathnam, and M. Ehsani, "Advantages of switched reluctance motor applications to EV and HEV: design and control issues," *IEEE Trans. Ind. Appl.*, vol. 36, no. 1, pp. 111-121, Jan./Feb. 2000.

[16] X.D.Xue, K.W.E Cheng, T.W. Ng, N.C. Cheung, "Multi-objective optimization design of in-wheel switched reluctance motors in electric vehicles," *IEEE Trans. Ind. Electron.*, vol.57, no.9, pp.2980-2987, Sept. 2010.

[17] S. Wang, Q. Zhan, Z. Ma, and L. Zhou, "Implementation of a 50-kW four-phase switched reluctance motor drive system for hybrid electric vehicle," *IEEE Trans. Magn.*, vol. 41, no. 1, pp. 501-504, Jan. 2005.

[18] K. M. Rahman, B. Fahimi, G. Suresh, A. V. Rajarathnam, and M. Ehsani, "Advantages of switched reluctance motor applications to EV and HEV: design and control issues," *IEEE Trans. Ind. Appl.*, vol. 36, no. 1, pp. 111-121, Jan./Feb. 2000.

[19] S. Wang, Q. Zhan, Z. Ma, and L. Zhou, "Implementation of a 50-kW four-phase switched reluctance motor drive system for hybrid electric vehicle," *IEEE Trans. Magn.*, vol. 41, no. 1, pp. 501-504, Jan. 2005.

[20] Z. Q. Zhu, and D. Howe, "Electrical machines and drives for electric, hybrid, and fuel cell vehicles," *Proceedings of the IEEE*, vol. 95, no. 4, pp. 746-765, Apr. 2007.

[21] B. Bilgin, A. Emadi, and M. Krishnamurthy, "Comprehensive Evaluation of the Dynamic Performance of a 6/10 SRM for Traction Application in PHEVs," *IEEE Trans. Ind. Electron.*, vol. 60, no. 7, pp. 2564-2575, Jul. 2013.

[22] M. Krishnamurthy, C. S. Edrington, A. Emadi, P. Asadi, M. Ehsani, and B. Fahimi, "Making the case for applications of switched reluctance motor technology in automotive products," *IEEE Trans. Power Electron.*, vol. 21, no. 3, pp. 659-675, May 2006.

[23] A. Emadi, Y. J. Lee, and K. Rajashekara, "Power electronics and motor drives in electric, hybrid electric, and plug-in hybrid electric vehicles," *IEEE Trans. Ind. Electron.*, vol. 55, no. 6, pp. 2237–2245, Jun. 2008.

[24] A. J. Forsyth and G. Calderon-Lopez. "Sampled-data analysis of the dual-interleaved boost converter with interphase transformer". *IEEE Trans. Power Electron.*, vol. 27, no. 3, pp.1338–1346 Mar. 2012.

[25] S. Haghbin, S. Lundmark, M. Alakula, and O. Carlson, "Grid-connected integrated battery chargers in vehicle applications: Review and new solution," *IEEE Trans. Ind. Electron.*, vol. 60, no. 2, pp. 459–473, Feb. 2013.

[26] J. D. Santiago et al., "Electrical motor drivelines in commercial allelectric vehicles: A review," *IEEE Trans. Veh. Technol.*, vol. 61, no. 2, pp. 475–484, Feb. 2012.

[27] S. Haghbin, S. Lundmark, M. Alakula, and O. Carlson, "An isolated highpower integrated charger in electrified-vehicle applications," *IEEE Trans. Veh. Technol.*, vol. 60, no. 9, pp. 4115–4126, Nov. 2011.

[28] I. Subotic, E. Levi, M. Jones, and D. Graovac, "Multiphase integrated onboard battery chargers for electrical vehicles," in Proc. EPE Appl. Conf., Lille, France, 2013, pp. 1–10.

[29] M. Budhia, J. T. Boys, G. A. Covic, C.U. Huang, "Development of a single-sided flux magnetic coupler for electric vehicle IPT charging systems," *IEEE Trans. Industrial Electronics*, vol.60, no.1, pp.318-328, Jan. 2013.

[30] A. Khaligh, S. Dusmez, "Comprehensive topological analysis of conductive and inductive charging solutions for plug-in electric vehicles," *IEEE Trans. Vehicular Technology*, vol.61, no.8, pp.3475-3489, Oct. 2012.

[31] C. J. Shin, J. Y. Lee, "An electrolytic capacitor-less bi-directional EV on-board charger using harmonic modulation technique," *IEEE Trans. Power Electron.*, vol.29, no.10, pp. 5195-5203, Oct. 2013.

[32] M. Barnes and C. Pollock, “Forward converters for dual voltage switched reluctance motor drives,” *IEEE Trans. Power Electron.*, vol. 16, no. 1, pp. 83–91, Jan. 2001.

[33] Y.J. Lee, A. Khaligh, A. Emadi, “Advanced integrated bidirectional AC/DC and DC/DC converter for plug-in hybrid electric vehicles,” *IEEE Trans. Veh. Technol.*, vol.58, no.8, pp.3970-3980, Oct. 2009.

[34] C. Liaw and H. Chang, “An integrated driving/charging switched reluctance motor drive using three-phase power module,” *IEEE Trans. Ind. Electron.*, vol. 58, no. 5, pp. 1763–1775, May 2011.

[35] H. Plesko, J. Biela, J. Luomi, and J. Kolar, “Novel concepts for integrating the electric drive and auxiliary DC–DC converter for hybrid vehicles,” *IEEE Trans. Power Electron.*, vol. 23, no. 6, pp. 3025–3034, Nov. 2008.

[36] K. T. Weng and C. Pollock, “Low-cost battery-powered switched reluctance drives with integral battery-charging capability,” *IEEE Trans. Ind. Appl.*, vol. 36, no. 6, pp. 1676–1681, Nov./Dec. 2000.

[37] I. Subotic, N. Bodo, E.Levi, and M. Jones, “Onboard integrated battery charger for EVs using an asymmetrical nine-phase machine,” *IEEE Trans. Ind. Electron.*, vol. 62, no. 5, pp.3285–3295, May. 2015.

[38] S. Haghbin, K. Khan, S. Zhao, M. Alakula, S. Lundmark, O. Carlson, “An integrated 20-kW motor drive and isolated battery charger for plug-in vehicles,” *IEEE Trans. Power Electron.*, vol.28, no.8, pp.4013-4029, Aug. 2013.

[39] Chang, H.C.; Liaw, C.M., “Development of a compact switched-reluctance motor drive for EV propulsion with voltage-boosting and PFC charging capabilities,” *IEEE Trans. Veh. Technol*., vol.58, no.7, pp.3198-3215, Sept. 2009.

[40] W. Qian, H. Cha, F. Z. Peng and L. M. Tolbert, "55-kW Variable 3X DC-DC Converter for Plug-in Hybrid Electric Vehicles," *IEEE Trans. Power Electron.*, vol. 27, no. 4, pp. 1668-1678, April 2012.

[41] C. Gan, J. Wu, Y. Hu, S. Yang, W. Cao and J. M. Guerrero, "New Integrated Multilevel Converter for Switched Reluctance Motor Drives in Plug-in Hybrid Electric Vehicles With Flexible Energy Conversion," *IEEE Trans. Power Electron.*, vol. 32, no. 5, pp. 3754-3766, May 2017.